

# Detecting Dark Matter with Superconducting Nanowires

Yonit Hochberg<sup>1,\*</sup>, Ilya Charaev<sup>2,†</sup>, Sae-Woo Nam<sup>3,‡</sup>, Varun Verma<sup>3,§</sup>, Marco Colangelo<sup>2,¶</sup> and Karl K. Berggren<sup>2,\*\*</sup>

<sup>1</sup>*Racah Institute of Physics, Hebrew University of Jerusalem, Jerusalem 91904, Israel*

<sup>2</sup>*Massachusetts Institute of Technology, Department of Electrical Engineering and Computer Science, Cambridge, MA, USA and*

<sup>3</sup>*National Institute of Standards and Technology, Boulder, CO, USA*

We propose the use of superconducting nanowires as both target and sensor for direct detection of sub-GeV dark matter. With excellent sensitivity to small energy deposits on electrons, and demonstrated low dark counts, such devices could be used to probe electron recoils from dark matter scattering and absorption processes. We demonstrate the feasibility of this idea using measurements of an existing fabricated tungsten-silicide nanowire prototype with 0.8-eV energy threshold and 4.3 nanograms with 10 thousand seconds of exposure, which showed no dark counts. The results from this device already place meaningful bounds on dark matter-electron interactions, including the strongest terrestrial bounds on sub-eV dark photon absorption to date. Future expected fabrication on larger scales and with lower thresholds should enable probing new territory in the direct detection landscape, establishing the complementarity of this approach to other existing proposals.

## INTRODUCTION

Dark matter (DM) is one of the most important unsolved mysteries of the Universe. Focus on the Weakly Interacting Massive Particle (WIMP) paradigm has guided experimental searches for decades. Traditional methods searching for such weak-scale DM in the laboratory via nuclear recoils have made tremendous progress in probing DM with mass above the GeV-scale, but typically make poor targets for detection of sub-GeV DM that goes beyond the WIMP paradigm. As the WIMP parameter space continues to be covered without discovery of DM, new ideas to search for lighter DM are of the essence.

Indeed, recent years have seen a surge of such new ideas emerge. These include the use of atomic excitations [1], electron recoils in semiconductors [1–4], 2-dimensional targets such as graphene [5] and carbon nanotubes [6], color centers [7] and scintillators [8], which can be sensitive to MeV-scale DM masses. Sub-MeV DM can further be probed by superconductors [9–11], Dirac materials [12], superfluid helium [13, 14] and polar crystals [15, 16]. The proposed experimental designs for each distinct target material differ from one another, with a variety of sensor technology employed across designs, including the use of CCDs, TESs, MKIDs and G-FETs coupled to a target.

Quantum information science has been breaking new ground in sensor technology, with superconducting nanowires a now established and burgeoning field [17–19]. Some of these nanowires have sub-eV energy sensitivity, which allows them to be used as single-excitation detectors. The recent emphasis on development of such low-threshold, ultra-fast and low-noise single-photon detectors for photonic quantum information applications [20, 21] promises a radical improvement in the search for DM. The advent of superconducting nanowire detectors, which currently have fewer than 10 dark counts per day [22] and have demonstrated sensitivity from the mid-infrared [23] to the ultraviolet wave-

length band [22], provides an opportunity to search for rare low-energy deposits of DM via scattering or absorption processes.

Here we propose and perform initial experiments using this technology as both the target for DM interactions with electrons and the sensor with which to detect these interactions. Depending on the energy thresholds reached in these devices—nanowires with sub-eV thresholds have already experimentally realized [23]—sensitivity to low-mass DM can be achieved. Energy deposits of order a few eV and above can further allow for directional detection of DM via a stacked geometry, which would serve as a powerful discriminator between signal and background.

In this letter, we begin by describing the basic detection process in these devices. We then describe an existing prototype nanowire and report on how it can be used to extract new bounds on DM interactions with electrons both in scattering and absorption processes. Our projections for future reach of superconducting nanowires into the DM parameter space follow. We conclude with discussion of impact, remaining issues and possible future work.

## CONCEPT

Superconducting nanowires are a rapidly developing technology with applications ranging from space communications [24, 25], to LIDAR [26, 27], to quantum-information science [28]. With sub-eV energy sensitivity [23],  $\sim 10^{-4}$  counts per second (cps) dark count rates [22], and spatial discrimination ability [29], superconducting-nanowire single-photon detectors (SNSPDs) provide an excellent candidate for detecting DM. SNSPDs are fabricated by using superconducting films a few-nm thick on a variety of substrates, with widths between 30 nm and 200 nm using electron-beam lithography and reactive ion etching. SNSPDs are typi-

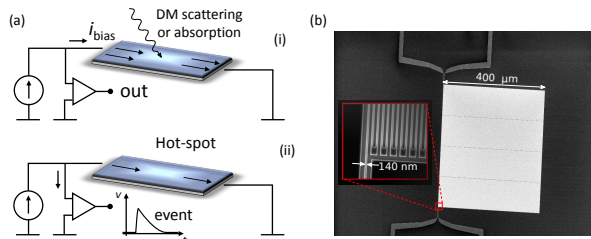


FIG. 1. (a) Schematic depiction of the operating principle of SNSPDs: (i) The detector is biased at a current close to the critical value. (ii) When the energy is absorbed by the nanowire, the electrons depart from equilibrium and diffuse out of the formed hot-spot. A resistive region formed across the nanowire then leads to a measurable voltage pulse in the readout. (b) The SEM image of the prototype WSi device after fabrication. The active area is 400 by 400  $\mu\text{m}^2$ . Nanowires are consistently connected to two contact pads.

cally fabricated into a planar meander structures covering tens to hundreds of square micrometers [30]. The device operating principle is straightforward: when cooled below the superconducting transition temperature and biased with a sufficiently high current, the energy deposited by an incident particle can cause the transition of a portion of the nanowire into the normal (resistive, non-superconducting) state. This appearance of a resistive region in the current-biased nanowire results in voltage pulses with typical amplitudes of  $\sim 1$  mV (depending on the amplifier's input impedance), and durations of a few to tens of nanoseconds. A schematic depiction of the device operation is shown in Fig. 1(a). These detectors have demonstrated dark count rates as low as  $1 \times 10^{-4}$  cps [22], making them particularly interesting for sensing rare events.

We therefore propose the use of SNSPDs for direct detection of DM. They can be used as both the target material with which the DM interacts, as well as the sensitive sensor measuring this interaction. Large target mass can be achieved via large arrays combined with multiplexing [31], without disturbing the excellent energy threshold of these devices nor their low-noise character.

A useful rule-of-thumb regarding the connection between the energy threshold of the device versus the DM mass that it can probe is as follows. In a DM scattering process off a target, the maximal energy deposited is the entire kinetic energy the particle is carrying  $\sim m_{\text{DM}} v_{\text{DM}}^2$ , with  $m_{\text{DM}}$  and  $v_{\text{DM}}$  the DM mass and velocity, respectively. Since the DM velocity around us is of order  $10^{-3}$  in natural units (where  $c = \hbar = 1$ ), a given system sensitive to energy deposits of  $E_{\text{D}}$  or larger can probe DM masses  $10^6$  larger than  $E_{\text{D}}$  via the scattering process,  $E_{\text{D}}^{\text{scat}} \sim 10^{-6} m_{\text{DM}}$ . If instead the DM particle is absorbed by the target, it deposits its entire mass-energy, meaning that the same target system is sensitive

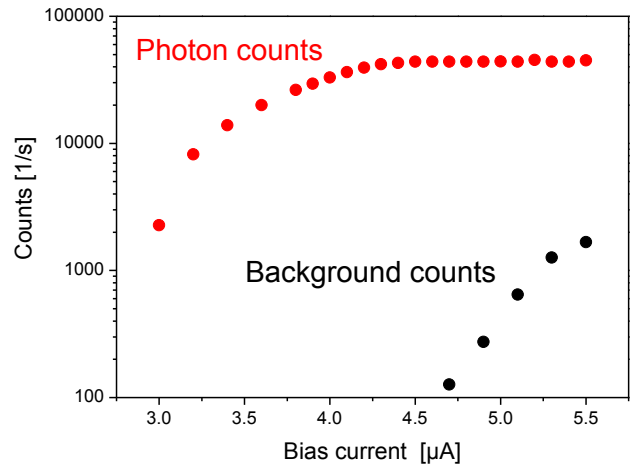


FIG. 2. The photon (red) and background (black) counts as a function of the absolute bias current, exhibited by the prototype WSi device tested in a fiber-coupled package at 300 mK.

to  $E_{\text{D}}^{\text{abs}} \sim m_{\text{DM}}$  via absorption processes.

For DM scattering with electrons in the SNSPDs, devices with eV-scale thresholds can thus probe DM masses of MeV and above. In this mass range, several proposed other targets exist in the literature (see, *e.g.*, Ref. [32] for a recent community report). The reach of the SNSPDs can be comparable to or better than these other targets, depending on exposure size and duration, and is complementary to other approaches. The SNSPDs, however, offer the advantage of possible directionality of the signal: with energy deposits of a few eV and above, the electrons are likely to be ejected from the material, and could then hit multiple layers of SNSPD arrays. If it is found that the ejected electron from the superconductor tracks the direction of the incoming DM particle [33], then reproducing the direction of the outgoing electron via the stacked geometry and the SNSPD's spacial discrimination power would inform us about the directionality of the signal. This could also help discriminate signal from background. Similar use of directionality from a stacked configuration has been suggested for use of in graphene targets [5].

As the threshold of the device is lowered to sub-eV energies, lower DM masses can be probed, with  $\mathcal{O}(\text{meV})$  energy deposits above the superconducting gap corresponding to  $\mathcal{O}(\text{keV})$  DM masses. Indeed, nanowires that exhibit sensitivity to  $5 \mu\text{m}$  wavelength photons, corresponding to an energy threshold of  $\sim 250$  meV, have been demonstrated [23], and it is likely that further technology developments could push the energy sensitivity to  $10 \mu\text{m}$  or even beyond. As we will show, the reach of the SNSPDs into the sub-MeV DM mass range is substantial, and can provide excellent results even with very small target masses, which can be constructed on rela-

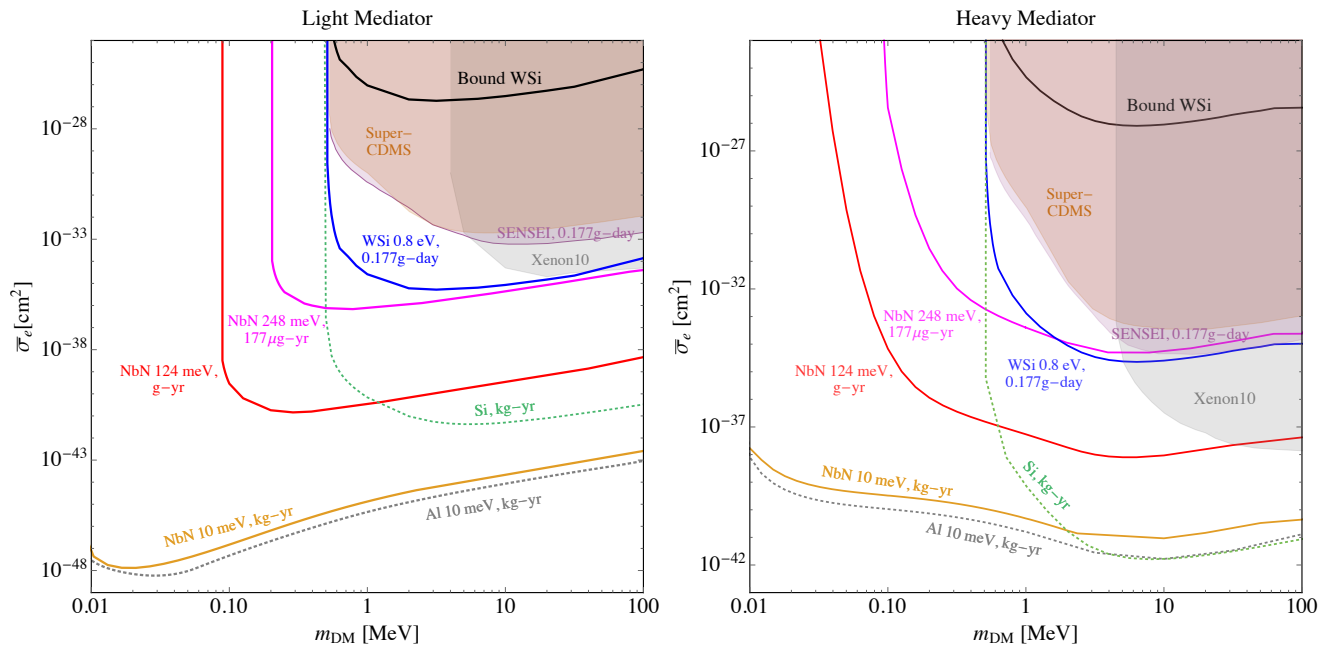


FIG. 3. Expected reach for DM-electron scattering via a light (*left panel*) and heavy (*right panel*) mediator as a function of DM mass. The solid black curve labeled ‘Bound WSi’ indicates the new bound placed by our prototype device with 4.3 ng exposed for 10,000 seconds. Other solid curves indicate our 95% C.L. projected reach for either NbN or WSi targets, with various exposures and thresholds. Also shown are the existing constraints from Xenon10 [2] (shaded gray), SuperCDMS [34] (shaded red) and SENSEI [35] (shaded purple), as well as the projected reach for a kg-yr exposure of a silicon target [36] (dotted green) and superconducting bulk aluminum with a 10 meV threshold [9, 10] (dotted gray). For clarity, 177  $\mu\text{g}$  corresponds to a 10 by 10  $\text{cm}^2$  area of NbN at 4 nm thickness and a 50% fill factor, and 248 (124) meV threshold corresponds to a 5 (10)  $\mu\text{m}$  wavelength.

tively short time scales.

Additionally, as we will show, absorption of DM in the sub-eV and above mass range is similarly possible via SNSPDs, providing an important complementary probe to *e.g.* existing stellar constraints.

### EXISTING PROTOTYPE DEVICE

Having presented the basic concept of detection via SNSPDs, we now describe an existing prototype device and how measurements of its performance already place bounds on DM scattering and absorption.

Fig. 1(b) is a scanning electron micrograph (SEM) of the prototype tungsten silicide (WSi) device after fabrication. The active device area was 400 by 400  $\mu\text{m}^2$ , and the nanowire was connected to external circuitry via two contact pads. The width of the nanowires was 140 nm with a pitch of 340 nm. The thickness of the WSi film was 7 nm, and the resulting mass is 4.3 ng. Further details of the device design and fabrication are provided in the Appendix.

The switching current of the device  $I_C$  was 5.5  $\mu\text{A}$  was measured at 300 mK by sweeping the current from a 50  $\Omega$  impedance source. Fig. 2 shows the dependence of the count rate on the absolute bias current for this

400 by 400  $\mu\text{m}^2$  large-area SNSPD at 1550 nm wavelength ( $\sim 0.8$  eV). When the detector was illuminated, the count rate rose at a bias current of 3  $\mu\text{A}$ . Counts initially grew with the current and the device saturated at a bias current of 4.5  $\mu\text{A}$ . At this bias current, the count rate with the laser light turned off (background count rate) was below 100 cps. The maximum background count rate was measured at a point just below the transition to the resistive state, at  $10^3$  cps.

The measurement of dark counts was performed in an apparatus with several layers of shielding and the optical fiber connection removed, at 4.5  $\mu\text{A}$  of bias current for  $10^4$  s. No dark counts were observed over this period, suggesting a dark count rate below 100 counts per microsecond. These measurements will be used below to place bounds on DM interactions.

### REACH

Our results for the reach of superconducting nanowires into the parameter space of DM-electron scattering are shown in Fig. 3. We follow the analyses of Refs. [9, 10] for rate computation in superconducting targets, with the appropriate modifications to Fermi energies  $E_F$  and the density  $\rho$  of target materials that are typically used for

the superconductors of SNSPDs. Details of the scattering rate computation can be found in the Appendix. Our results for niobium nitride (NbN) and WSi targets use  $\rho_{\text{NbN}} = 8.4 \text{ g/cm}^3$  and  $\rho_{\text{WSi}} = 9.3 \text{ g/cm}^3$ , respectively, and in both cases we use  $E_F = 7 \text{ eV}$ . (We note that while the Fermi surface of WSi is not a perfect sphere, the calculations performed here are intended to provide a proxy to guide future experiments; we have thus assumed a spherical Fermi surface in the case of WSi.)

The left panel shows the reach for scattering via a light mediator, with the commonly used reference momentum  $q_{\text{ref}} = \alpha m_e$  defining the reference cross section  $\bar{\sigma}_e$ , while the right panel shows the reach when scattering via a heavy mediator (see Appendix for all definitions). The solid colored curves show the 95% Confidence Level (C.L.) projected reach, corresponding to 3 signal events, for SNSPDs with various amounts of exposures and thresholds, assuming a dynamic range of 3 orders of magnitude. We also show the projected reach for a kg-year exposure of a silicon target with single-electron sensitivity [36] and of an aluminum target with a 10 meV threshold TES [9, 10], along with constraints from the Xenon10 [2], SENSEI [35] and SuperCDMS [34] experiments.

The 95% C.L. bound on DM-electron scattering placed by the 4.3 nanogram prototype WSi device with the 0.8 eV energy threshold presented in this work, which showed no dark counts in 10 thousand seconds of exposure, is shown by the black solid curve. While the bound from this prototype nanowire on DM-electron scattering is not yet competitive with those from the other experiments, it is impressively placed using a tiny mass-time exposure on a surface run. For comparison, the projected reach of a WSi target with an exposure similar to that of the SENSEI data, 0.177g-day, is also shown, demonstrating the strength of our proposal. As is evident, larger exposures combined with low thresholds will enable superconducting nanowires to quickly probe uncharted parameter space of DM scattering.

In addition to probing DM-electron scattering, SNSPDs can simultaneously probe absorption of relic particles that interact with electrons. As an example, we consider a relic dark photon that is kinetically mixed with the ordinary photon. Effectively, such a dark photon interacts with electrons in a similar manner to the photon, but with the interaction suppressed by the size of the kinetic mixing,  $\kappa$  (see Appendix for further details).

Our results for relic dark photon absorption in SNSPDs are shown in Fig. 4. We use low-energy photon absorption data for NbN [23] and WSi [42, 43], and translate it to the expected reach on the size of kinetic mixing  $\kappa$  between the photon and dark photon field strengths as a function of the dark photon mass  $m_V$ . Details of the absorption rate computation can be found in the Appendix. We show the resulting 95% C.L. expected reach, corresponding to 3 signal events, for a kg-year exposure of

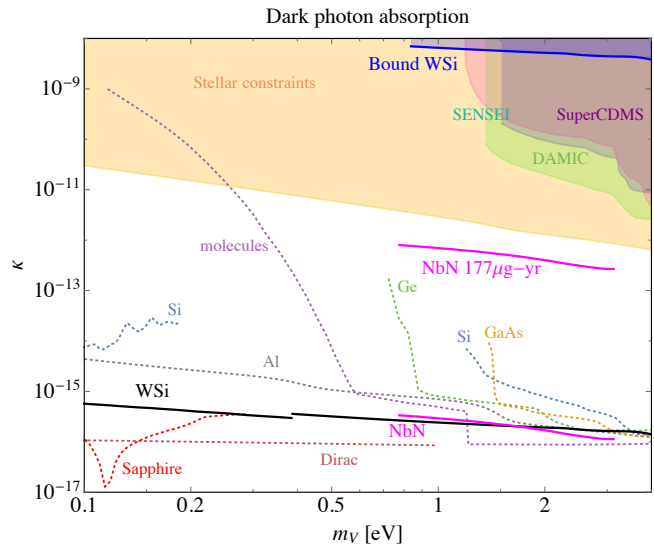


FIG. 4. Expected reach for absorption of relic dark photons. The solid blue curve labeled ‘Bound WSi’ indicates the new bound placed by our prototype device in this work, which showed no dark counts in 4.3 ng over  $10^4$  seconds. The projected reach for a NbN target SNSPD with  $177 \mu\text{g-yr}$  (corresponding to a 10 by 10  $\text{cm}^2$  area with 4 nm thickness and a 50% fill factor), and kg-year exposures is shown (solid magenta curves); NbN reach into lower masses than depicted should be possible and can be estimated from lower energy data should it become available. Also shown is our projected reach for a kg-yr exposure of a WSi SNSPD (solid black). The reach for a kg-yr exposure of aluminum superconductors [11], semiconductors such as germanium and silicon [37], Dirac materials [12], molecules [38] and polar crystals such as GaAs and Sapphire [16] are given as well (dotted curves). Constraints from stellar emission [39, 40] are indicated (shaded orange), along with terrestrial constraints from SuperCDMS [34] (shaded purple), DAMIC [41] (shaded green) and SENSEI [35] (shaded turquoise). Unless otherwise stated, projected reach refers to kg-yr exposure.

NbN and WSi target SNSPDs. For NbN, we additionally present the reach of a  $177 \mu\text{g-yr}$  exposure; we further note that reach into lower masses than depicted is possible and can be estimated should lower energy data become available. Also shown are constraints from SuperCDMS [34], DAMIC [41] and SENSEI [35], along with stellar emission constraints [39, 40]. The projected reach for kg-year exposures of germanium and silicon [37], superconducting aluminum [11], Dirac materials [12], polar crystals such as GaAs and shapphire [16] as well as molecular targets [38] are likewise indicated.

The 95% C.L. bound on relic dark photons placed by the data of the 4.3 ng prototype WSi device in  $10^4 \text{ s}$  with a 0.8 eV threshold, presented in this work, is shown by the solid blue curve. Remarkably, despite the small device size and short exposure time of our experiment, it places the strongest terrestrial constraint to date on dark photons with sub-eV masses.

## SUMMARY

We have proposed the use of superconducting nanowires as sensitive targets and detectors for light dark matter, and demonstrated the power of this approach. We have found that absorption of bosonic DM with masses above the superconducting gap of  $\mathcal{O}(\text{meV})$  and scattering of DM in the keV to GeV mass range are both promising and complementary to other existing proposals in these mass ranges. An existing prototype nanowire already places meaningful bounds on the parameter space, including the strongest terrestrial constraints to date on dark photon absorption in the sub-eV to few-eV mass range.

The results presented here suggest that further work, both theoretical and experimental, is warranted to determine the viability of using SNSPDs for this goal. In the Appendix, we discuss several issues raised by our results, in particular: (i) what are the ideal device characteristics that should be targeted; and (ii) what are the prospects for scaling the detectors to masses large enough to substantially extend the reach of current searches.

With low thresholds and low dark count rates, superconducting nanowires have the potential to impact the direct detection landscape on relatively short time scales. We hope this work serves as a stimulant for broad cooperation between the quantum information and fundamental physics communities, such that meaningful progress can rapidly be made towards understanding the basic constituents of nature.

**Acknowledgments.** We thank Tom Dvir, Nadav Katz and Hadar Steinberg for useful discussions that led to this work, and Eric David Kramer and Eric Kuflik for many helpful discussions. We thank Phil Mauskopf for providing the cryogenic amplifiers used in this experiment. KKB thanks Asimina Arvanitaki and Ken van Tilburg for helpful discussions. The work of YH is supported by the Israel Science Foundation (grant No. 1112/17), by the Binational Science Foundation (grant No. 2016155), by the I-CORE Program of the Planning Budgeting Committee (grant No. 1937/12), by the German Israel Foundation (grant No. I-2487-303.7/2017), and by the Azrieli Foundation. The work of KKB was supported in part by the DOE under the QuantiSED program, grant number de-sc0019129.

## APPENDIX

### Prototype Device Details

Here we provide the technical details of the prototype device used in this paper to set new bounds on dark matter scattering and absorption. The device used in the experiment was fabricated from 7-nm thick WSi film which was deposited on a silicon substrate at room temperature

by using an RF co-sputtering technique [44]. Additionally, a thin 2-nm Si layer was *in situ* deposited on top of the WSi film to prevent oxidation of the superconductor. The critical temperature of the sputtered film was measured at the point where  $R = R_{20}/2$  ( $R_{20}$  is the resistance at 20 K) and was found to be 4.08 K.

To pattern the nanowires, electron-beam lithography was used with high-resolution positive e-beam resist. The ZEP 520 A resist was spin coated onto the chip at 5000 rpm which ensured a thickness of 335 nm. The resist was exposed to a 125 keV electron beam with an area dose density of  $500 \mu\text{C}/\text{cm}^2$ . After exposure, the resist was developed by submerging the chip in O-xylene for 80 s with subsequent rinsing in the 2-propanol stopper. The ZEP 520 A pattern was then transferred to the WSi by reactive ion etching in  $\text{CF}_4$  at 50 W for 5 minutes.

To electrically and optically characterize the fabricated device, we designed an experimental setup using a single shot type He-3 cryostat. The device was mounted on the sample holder using a contact glue. The holder was placed on a 300-mK cold stage and was shielded to reduce the effect of background radiation on the detector noise. A low-temperature bias tee decoupled the high-frequency path from the DC bias path. The high-frequency signal was carried out of the cryostat by stainless-steel rigid coaxial cables, while DC bias was provided via a pair of twisted wires connected to a low-noise voltage source. The signal was amplified at the 4 K stage by a cryogenic low-noise amplifier with the total gain of 56 dB and then sent to a pulse counter. The optical single mode fiber feeds light from the 1550-nm CW laser into the cryogenic apparatus through a vacuum feedthrough and is mounted on a stage above the sample surface. An optical attenuator was used to ensure the single-photon counting regime.

### Dark Matter Scattering Rate

Here we review the scattering rate of dark matter with electrons in a superconducting target, used to obtain our parameter space reach plot in Fig. 3. Denoting the 4-momentum of the DM initial and final state particle by  $P_1$  and  $P_3$ , the initial and final states of the electron by  $P_2$  and  $P_4$ , and the momentum transfer  $q = (E_D, \mathbf{q})$ , the scattering rate is given by [9, 10]

$$\langle n_e \sigma v_{\text{rel}} \rangle = \int \frac{d^3 p_3}{(2\pi)^3} \frac{\langle |\mathcal{M}|^2 \rangle}{16E_1 E_2 E_3 E_4} S(E_D, |\mathbf{q}|), \quad (1)$$

$$S(E_D, |\mathbf{q}|) = 2 \int \frac{d^3 p_2}{(2\pi)^3} \frac{d^3 p_4}{(2\pi)^3} (2\pi)^4 \delta^4(P_1 + P_2 - P_3 - P_4) \times f_2(E_2)(1 - f_4(E_4)),$$

where  $E_D$  is the deposited energy,  $\langle |\mathcal{M}|^2 \rangle$  is the squared scattering matrix element summed and averaged over spin, and  $f_i(E_i) = [1 + \exp(\frac{E_i - \mu_i}{T})]^{-1}$  is the Fermi-Dirac distribution of the electrons at temperature  $T$ , with  $\mu_i$

the chemical potential (equal to the Fermi energy at zero temperature). The total rate (in number of events, per unit time per unit mass) is then

$$E_D \frac{dR_{\text{DM}}}{dE_D} = \int dv_{\text{DM}} f_{\text{MB}}(v_{\text{DM}}) E_D \frac{d\langle n_e \sigma v_{\text{rel}} \rangle}{dE_D} \frac{1}{\rho} \frac{\rho_{\text{DM}}}{m_{\text{DM}}} \quad (2)$$

where  $\rho$  is the mass density of the target material,  $\rho_{\text{DM}} = 0.3 \text{ GeV/cm}^3$  is the DM mass density, and  $v_{\text{rel}}$  is the relative velocity between the electrons and the DM. The DM velocity distribution  $f_{\text{MB}}(v_{\text{DM}})$  is taken to be a modified Maxwell Boltzmann distribution with root mean square velocity  $v_0 = 220 \text{ km/s}$ , with a cut-off at the escape velocity  $v_{\text{esc}} = 500 \text{ km/s}$ .

The scattering cross section of DM and electrons is related to the matrix element squared via  $\sigma_{\text{scatter}} = \frac{\langle |\mathcal{M}|^2 \rangle}{16\pi E_1 E_2 E_3 E_4} \mu_{e\text{DM}}^2$ , with  $\mu_{e\text{DM}}$  the reduced DM-electron mass, and we define a reference cross section  $\bar{\sigma}_e$  as is common in the literature with fixed momentum transfer  $q_{\text{ref}} = \alpha m_e$ . Namely,

$$\bar{\sigma}_e \equiv \frac{\mu_{e\text{DM}}^2}{16\pi m_{\text{DM}}^2 m_e^2} \langle |\mathcal{M}(q)|^2 \rangle_{|q^2 = \alpha^2 m_e^2}, \quad (3)$$

$$\langle |\mathcal{M}(q)|^2 \rangle = \langle |\mathcal{M}(q)|^2 \rangle_{|q^2 = \alpha^2 m_e^2} \times |F_{\text{DM}}(q)|^2, \quad (4)$$

with  $F_{\text{DM}}(q)$  the form factor that encompasses the momentum dependence of the cross section.  $\bar{\sigma}_e$  is then equal to the non-relativistic DM-electron elastic cross section with the reference momentum transfer  $q_{\text{ref}} = \alpha m_e$ . For scattering processes that occur via the exchange of a heavy mediator between the DM and the electrons,  $F_{\text{DM}} = 1$ , while for a light mediator exchange,  $F_{\text{DM}} = q_{\text{ref}}^2/q^2$ .

Our results for the reach of superconducting nanowires into the reference cross section  $\bar{\sigma}_e$  of DM-electron scattering parameter space, for heavy and light mediators, are shown in Fig. 3.

### Dark Photon Absorption Rate

Here we review how we obtain the absorption rate of a relic dark photon in a given material, which leads to our Fig. 4, via the optical response of the material. We consider the Lagrangian of a dark photon with an induced kinetic mixing with the photon (sourced by a kinetic mixing with the hypercharge gauge boson),

$$\mathcal{L} \supset -\frac{\kappa}{2} F_{\mu\nu} V^{\mu\nu}, \quad (5)$$

where  $F^{\mu\nu}$  and  $V^{\mu\nu}$  are the field strengths for the photon  $A$  and dark photon  $V$ , respectively:  $F_{\mu\nu} = \partial_\mu A_\nu - \partial_\nu A_\mu$ , and  $V^{\mu\nu}$  is similarly defined with the replacement  $A^\mu \rightarrow V^\mu$  (here  $\mu, \nu = 0, \dots, 4$  are Lorentz indices). The effective mixing angle in a medium is given by

$$\kappa_{\text{eff}}^2 = \frac{\kappa^2 m_V^4}{[m_V^2 - \text{Re} \Pi(m_V)]^2 + [\text{Im} \Pi(m_V)]^2}, \quad (6)$$

where  $m_V$  is the mass of the dark photon, and  $\Pi$  is the polarization tensor of the material, related to the optical conductivity of the material  $\hat{\sigma}$  through

$$\Pi(\omega) \approx -i\hat{\sigma}\omega, \quad (7)$$

with the conductivity related to the complex index of refraction  $\hat{n}$  by  $\hat{n}^2 = 1 + i\hat{\sigma}/\omega$ . We relate the absorption of dark photons to that of ordinary photons to obtain the absorption rate for dark photons in the given material. For absorption processes, the deposited energy is  $\omega \approx m_V$ . The result is that the absorption rate in counts per unit mass per unit time is

$$R = \frac{1}{\rho} \frac{\rho_{\text{DM}}}{m_V} \kappa_{\text{eff}}^2 \text{Re} [\hat{\sigma}(m_V)], \quad (8)$$

where  $\kappa_{\text{eff}}^2$  is given by Eq. (6),  $\rho$  is the mass density of the target and  $\rho_{\text{DM}} = 0.3 \text{ GeV/cm}^3$  is the DM mass density, as before.

Our results for the reach of superconducting nanowires into the parameter space of dark photon absorption are shown in Fig. 4.

### Detector Considerations

We now consider issues associated with scaling the detectors to larger areas, higher efficiencies, lower dark count rates and lower energies. All of these elements correspond directly to improved system reach. Here, we propose a metric that can be used to quickly compare detector technologies, and discuss the prospect of scaling that metric by increasing the detector area.

**Dark Counts Figure of Merit.** A useful figure of merit (FOM) for DM detection with these detectors is the product of the device area  $A$  with the detection efficiency  $\eta$  divided by the dark count rate (DCR),  $\text{FOM} = \eta A / \text{DCR}$ . This FOM is dependent on wavelength, bias current, and film thickness, but is still relevant when comparing within existing detector families where these parameters are held relatively constant. Recent work [22] has demonstrated a detector with  $\text{FOM} = 2.7 \times 10^{-5} \text{ m}^2/\text{cps}$  for 4 eV light measured at  $T = 800 \text{ mK}$ .

The main parameters available to optimize this FOM are the bias current, the film thickness, and the detector geometry/design. Typically, higher bias current will increase the efficiency, but would also potentially increase the DCR, thus an intermediate value is desirable. In addition, thicker films will result in increased mass, but at the expense of reduced efficiency. Additionally, lower-energy photons are likely to be detectable with reduced efficiency in a thicker film. These complicated trade-offs mean that the detector design space used here is unlikely to be optimal, and further improvements are possible.

**Scaling.** Any reasonable effort at DM detection based on the proposed technique will require larger areas of detector to be manufactured. Recent work from

Ref. [45] has suggested that nanometer-length-scale device widths may not be required in order to realize SNSPDs (more properly then, SSPDs, as the wires are no longer true ‘nanowires’). In that case, optical lithography could be used exclusively in their fabrication and as such mass production at the wafer scale of large-area devices would be quite viable. An academic laboratory could readily produce in the course of a year a thousand 200-mm-diameter wafers, resulting in a total detector mass of 1.3 g. An industrial effort could realize many times that number. At that point, the main challenge would be testing and packaging, rather than simply manufacture. With proper design, planning and resources, target masses in the kg-range may be feasible.

---

\* yonit.hochberg@mail.huji.ac.il

† charaev@mit.edu

‡ nams@boulder.nist.gov

§ varun.verma@boulder.nist.gov

¶ colang@mit.edu

\*\* berggren@mit.edu

- [1] R. Essig, J. Mardon, and T. Volansky, *Phys. Rev.* **D85**, 076007 (2012), arXiv:1108.5383 [hep-ph].
- [2] R. Essig, A. Manalaysay, J. Mardon, P. Sorensen, and T. Volansky, *Phys. Rev. Lett.* **109**, 021301 (2012), arXiv:1206.2644 [astro-ph.CO].
- [3] P. W. Graham, D. E. Kaplan, S. Rajendran, and M. T. Walters, *Phys. Dark Univ.* **1**, 32 (2012), arXiv:1203.2531 [hep-ph].
- [4] N. Kurinsky, T. C. Yu, Y. Hochberg, and B. Cabrera, (2019), arXiv:1901.07569 [hep-ex].
- [5] Y. Hochberg, Y. Kahn, M. Lisanti, C. G. Tully, and K. M. Zurek, *Phys. Lett.* **B772**, 239 (2017), arXiv:1606.08849 [hep-ph].
- [6] G. Cavoto, F. Luchetta, and A. D. Polosa, *Phys. Lett.* **B776**, 338 (2018), arXiv:1706.02487 [hep-ph].
- [7] R. Budnik, O. Chesnovsky, O. Slone, and T. Volansky, *Phys. Lett.* **B782**, 242 (2018), arXiv:1705.03016 [hep-ph].
- [8] S. Derenzo, R. Essig, A. Massari, A. Soto, and T.-T. Yu, *Phys. Rev.* **D96**, 016026 (2017), arXiv:1607.01009 [hep-ph].
- [9] Y. Hochberg, Y. Zhao, and K. M. Zurek, *Phys. Rev. Lett.* **116**, 011301 (2016), arXiv:1504.07237 [hep-ph].
- [10] Y. Hochberg, M. Pyle, Y. Zhao, and K. M. Zurek, *JHEP* **08**, 057 (2016), arXiv:1512.04533 [hep-ph].
- [11] Y. Hochberg, T. Lin, and K. M. Zurek, *Phys. Rev.* **D94**, 015019 (2016), arXiv:1604.06800 [hep-ph].
- [12] Y. Hochberg, Y. Kahn, M. Lisanti, K. M. Zurek, A. G. Grushin, R. Ilan, S. M. Griffin, Z.-F. Liu, S. F. Weber, and J. B. Neaton, *Phys. Rev.* **D97**, 015004 (2018), arXiv:1708.08929 [hep-ph].
- [13] K. Schutz and K. M. Zurek, *Phys. Rev. Lett.* **117**, 121302 (2016), arXiv:1604.08206 [hep-ph].
- [14] S. Knapen, T. Lin, and K. M. Zurek, *Phys. Rev.* **D95**, 056019 (2017), arXiv:1611.06228 [hep-ph].
- [15] S. Knapen, T. Lin, M. Pyle, and K. M. Zurek, *Phys. Lett.* **B785**, 386 (2018), arXiv:1712.06598 [hep-ph].
- [16] S. Griffin, S. Knapen, T. Lin, and K. M. Zurek, *Phys. Rev.* **D98**, 115034 (2018), arXiv:1807.10291 [hep-ph].
- [17] C. Natarajan, M. Tanner, and R. Hadfield, *Supercond. Sci. Technol.* **25**, 063001 (2012).
- [18] R. Hadfield, *Nature Photonics* **3**, 696–705 (2009).
- [19] F. Najafi *et al.*, *Quantum Science and Technology* **11**, 3 (2007).
- [20] H. Takesue, S. W. Nam, Q. Zhang, R. Hadfield, T. Honjo, K. Tamaki, and Y. Yamamoto, *Nature Photonics* **1**, 343–348 (2007).
- [21] B. Calkins *et al.*, *Opt. Express* **21**, 22657 (2013).
- [22] E. Wollman *et al.*, *Opt. Express* **25**, 26792 (2017).
- [23] F. Marsili *et al.*, *Nano letters* **12**, 4799 (2012).
- [24] M. E. Grein, O. Shatrovov, D. V. Murphy, B. S. Robinson, and D. Boroson, *Conference on Lasers and Electro-Optics (CLEO 2014)*, SM4J.4 (2014).
- [25] Y. P. Korneeva, D. Y. Vodolazov, A. V. Semenov, I. N. Florya, N. Simonov, E. Baeva, A. A. Korneev, G. N. Goltsman, and T. M. Klapwijk, *Conference on Lasers and Electro-Optics (CLEO 2014)*, SM4J.5 (2014).
- [26] A. McCarthy, N. J. Krichel, N. R. Gemmel, X. Ren, M. G. Tanner, S. N. Dorenbos, V. Zwiller, R. H. Hadfield, and G. S. Buller, *Opt. Express* **21**, 8904 (2013).
- [27] L. Chen *et al.*, *Acc. Chem. Res* **50**, 1400–1409 (2017).
- [28] C. M. Natarajan, M. M. Härtig, R. E. Warburton, G. S. Buller, R. H. Hadfield, B. Baek, S. W. Nam, S. Miki, M. Fujiwara, M. Sasaki, and Z. Wang, in *Quantum Communication and Quantum Networking*, edited by A. Sergienko, S. Pascazio, and P. Villoresi (Springer Berlin Heidelberg, Berlin, Heidelberg, 2010) pp. 225–232.
- [29] Q. Zhao *et al.*, *Nature Photonics* **11**, 247–251 (2007).
- [30] C. Lv *et al.*, *Supercond. Sci. Technol.* **30**, 115018 (2017).
- [31] E. A. Dauler, A. J. Kerman, B. S. Robinson, J. K. Yang, B. Voronov, G. Goltsman, S. A. Hamilton, and K. K. Berggren, *Journal of Modern Optics* **56**, 364 (2009).
- [32] M. Battaglieri *et al.*, (2017), arXiv:1707.04591 [hep-ph].
- [33] Y. Hochberg, E. D. Kramer, N. Kurinsky, and K. M. Zurek, work in progress.
- [34] R. Agnese *et al.* (SuperCDMS), *Phys. Rev. Lett.* **121**, 051301 (2018), arXiv:1804.10697 [hep-ex].
- [35] O. Abramoff *et al.* (SENSEI), (2019), arXiv:1901.10478 [hep-ex].
- [36] R. Essig, M. Fernandez-Serra, J. Mardon, A. Soto, T. Volansky, and T.-T. Yu, *JHEP* **05**, 046 (2016), arXiv:1509.01598 [hep-ph].
- [37] Y. Hochberg, T. Lin, and K. M. Zurek, *Phys. Rev.* **D95**, 023013 (2017), arXiv:1608.01994 [hep-ph].
- [38] A. Arvanitaki, S. Dimopoulos, and K. Van Tilburg, *Phys. Rev.* **X8**, 041001 (2018), arXiv:1709.05354 [hep-ph].
- [39] H. An, M. Pospelov, and J. Pradler, *Phys. Rev. Lett.* **111**, 041302 (2013), arXiv:1304.3461 [hep-ph].
- [40] H. An, M. Pospelov, J. Pradler, and A. Ritz, *Phys. Lett.* **B747**, 331 (2015), arXiv:1412.8378 [hep-ph].
- [41] A. Aguilar-Arevalo *et al.* (DAMIC), *Phys. Rev. Lett.* **118**, 141803 (2017), arXiv:1611.03066 [astro-ph.CO].
- [42] F. Marsili *et al.*, *Nano letters* **7**, 210–214 (2013).
- [43] I. Yamada, J. Nishii, and M. Saito, *Applied Optics* **47**, 4735 (2008).
- [44] B. Baeka, A. Lita, V. Verma, and S.-W. Nam, *Appl. Phys. Lett.* **98**, 251105 (2009).
- [45] Y. P. Korneeva, D. Y. Vodolazov, A. V. Semenov, I. N. Florya, N. Simonov, E. Baeva, A. A. Korneev, G. N. Goltsman, and T. M. Klapwijk, *Phys. Rev. Applied* **9**, 064037 (2018).